Available online at www.sciencedirect.com
SCIENCE DIRECT®
ELSEVIER
International Journal of Solids and Structures 41 (2004) 7091–7110
INTERNATIONAL JOURNAL OF SOLIDS and STRUCTURES
www.elsevier.com/locate/ijsolstr

Plastic dynamic breakup of a free–free beam subjected to impact at two free ends

J.L. Yang [a,*], X.H. Liu [a], Y.L. Hua [b]

[a] Solid Mechanics Research Center, Beijing University of Aeronautics and Astronautics, Beijing 100083, PR China
[b] Mechanics of Materials Group, China Agricultural University (East Campus), Beijing 100083, PR China

Received 10 October 2003; received in revised form 11 June 2004
Available online 20 July 2004

Abstract

The dynamic plastic failure characteristics of a free–free beam subjected to impact at its two free ends by moving concentrated masses are studied. Based on rigid, perfectly plastic (r-p-p) material idealization the complete solutions in closed form are obtained. Attention is focused on the permanent distribution of the curvature and the cross-sectional rotation along the axis of the beam, so as to predict the possible breakup cross-section in the beam. The results based on present r-p-p model are compared with those predicted by FEM analysis based on elastic, perfectly plastic (e-p-p) material idealization. It is shown that the agreement is good between the predictions of the r-p-p and e-p-p models on the cross-section positions with maximum rotation. The breakup of the impinged beam may occur on these positions most possibly.

Keywords: Free–free beam; Two point impact; Rigid perfectly plastic idealization; Failure region

1. Introduction

When flying in space, a vehicle is prone to attack by various kinds of projectiles. The damage resulting from impact may lead to failure of the vehicle. In most cases, due to the complexity of the vehicle structure, the analysis of the dynamic deformation behavior of vehicle fuselage by using accurate theoretical model is difficult. As a rough estimation of the failure characteristic of vehicle fuselage subjected to impact, some simple but effective methods can be adopted. For example, the long fuselage vehicle with relative small cross-section can be modeled approximately as a free–free beam in space or a free–free circular thin shell. When the kinetic energy of the projectile is sufficient large, the rigid, perfectly plastic approach can be employed to estimate the plastic deformation of the structure such as free–free beam or free–free circular shell. Actually, the dynamic plastic responses of free–free beams under impulsive loading have drawn some

* Corresponding author. Tel.: +86-1082317528; fax: +86-1082328719.
E-mail address: jlyang@buaa.edu.cn (J.L. Yang).

0020-7683/$ - see front matter © 2004 Elsevier Ltd. All rights reserved.
doi:10.1016/j.ijsolstr.2004.06.013

Nomenclature

c	the ratio of initial momentum of the two strikers defined in Eq. (11)
e_{01}, e_{02}	the non-dimensional initial dynamic energy of the two strikers, respectively, defined in Eq. (1)
e_p	the non-dimensional plastic dissipated work
G_1, G_2	the mass of the two strikers, respectively
g_1, g_2	the non-dimensional value of G_1 and G_2 respectively, defined in Eq. (1)
k_1, k_2	the curvature in segment AH_1 and BH_2, respectively
L	the length of half of the free–free beam
M_p	the fully plastic bending moment
m	the mass per unit length of the beam
S_1, S_2	length of segments AH_1 and BH_2, respectively
t	time
$\dot{u}_1$, $\dot{u}_2$	the non-dimensional velocity of impact points A and B, respectively
V_1, V_2	the velocity of free ends A and B, respectively
v_1, v_2	the non-dimensional value of V_1 and V_2 respectively, defined in Eq. (1)
V_{10}, V_{20}	the initial velocity of the two strikers, respectively
v_{10}, v_{20}	non-dimensional value of V_{10} and V_{20} respectively, defined in Eq. (1)
W_1, W_2	the transverse deflection of the neutral axis of the beam in segment AH_1 and BH_2, respectively
w_1, w_2	the non-dimensional transverse deflection, defined in Eq. (1)
X_1, X_2	the coordinate see Fig. 2
x_1, x_2	the non-dimensional coordinate of X_1 and X_2 respectively, defined in Eq. (1)
Greeks	
ξ	S_1/L
ς	S_2/L
τ	the non-dimensional time, defined in Eq. (1)
κ_1, κ_2	the non-dimensional curvature, defined in Eq. (1)
θ_1, θ_2	the rotation angle of the cross-section along AH_1 and BH_2 respectively
$\dot{\varphi}_1$, $\dot{\varphi}_2$	the non-dimensional angular velocity of segments AH and BH, respectively
$\dot{(\,)}$	$\frac{\mathrm{d}}{\mathrm{d}\tau}(\,)$
Subscript	
I	values at the end of Phase I
II	values at the end of Phase II

attentions over the past fifty years and several publications concerned with both experiment and theoretical studies can be found in Lee and Symonds (1952); Symonds (1953, 1985); Symonds and Leth (1954); Yang and Xi (2000); Woodward and Baxtex (1986); Yu et al. (1996) and Yu et al. (2000). Among them, few studies focused on the plastic failure of the free–free beams subjected to impact. Against the background of the breakup analysis of an aerospace vehicle fuselage, Jones and Wierzbicki (1987) studied the dynamic plastic failure of a free–free beam subjected to dynamic pressure pulse based on the r-p-p model. The exact theoretical solutions and a crude estimation of breakup of an aerospace vehicle fuselage have been given and discussion was made for the failure modes of free–free beams. It should be mentioned that most of the studies were only deal with the case when the load was symmetric about the mid-span of the beam, e.g. a concentrated load, or an impact at mid-span, or impulsive loading uniformly distributed along the beam.

Recently, Yang et al. (1998) examined the deformation mechanisms of a free–free beam subjected to step loading at any arbitrary location along its span. A complete map of deformation modes for various combination of the magnitude and the location of the load and the partitioning of the energy dissipation were described. However the study was still not directly concerned with plastic failure behavior for the beam. In respect to multi-point impact response, Ahmed et al. (2001) recently adopted Lagrangian finite element formulation to analyze the elastic–plastic behavior of a free–free beam subjected to low velocity impact at the center or at two points symmetrically on the beam. The instantaneous profile, stress and strain distribution and energy partitioning of the deformed beam were obtained.

It is known that the dynamic plastic behavior of structures subjected to intense dynamic loading can be simulated by employing finite element codes such as MSC-Dytran, ABAQUS, ADINA and the like. Instead of conducting a numerical simulation, however, this article hopes to adopt an analytical approach to reveal the plastic failure behavior of free–free beams subjected to unsymmetrical intense dynamic loading. As a specific study object, a free–free beam is impinged at its two free ends by strikers (G_1 and G_2). The left and right strikers may have different initial velocity and different mass so that the initial momentums of the two strikers are different. This indicates that the dynamic response becomes unsymmetrical about its center. In the present paper, a simple model based on the r-p-p material idealization is proposed to simulate the dynamic behavior of the impinged free–free beam, which is appropriate if the input energy is much large than the maximum elastic energy that can be stored in the structure (Symonds, 1967; Symonds and Frye, 1988). Especially, it is expected to obtain the reasonable prediction on the failure behavior of the beam through some simple formulations from present model.

2. Analysis

As shown in Fig. 1, an uniform free–free beam of length $2L$ and mass m per unit length, is struck at its two free ends A and B at the same time, $t = 0$, by two concentrate masses G_1 and G_2 traveling with initial speeds V_{10} and V_{20}, respectively. It is assumed that (i) the material of the beam is rigid, perfectly plastic (r-p-p) and time independent; (ii) both strikers G_1 and G_2 remain attached at the beam during the whole response after impact; (iii) during plastic deformation phase of the response, the deflections of the beam are small enough that the equations of motion for the segments of the beam may be formulated on the original configuration. According to the assumptions, at the instant the masses hit the free–free beam two traveling hinges are formed in it at A and B, and thereafter the response of the system consists of three phases. In the first phase, $0 \leqslant t \leqslant t_{\mathrm{I}}$, two traveling plastic hinges H_1 and H_2 move along the beam from the left free end and right free end respectively, as shown in Fig. 2, until they meet each other at point P_{I} on the way in the beam. In the second phase, $t_{\mathrm{I}} \leqslant t \leqslant t_{\mathrm{II}}$, there are two possible deformation mechanisms, i.e. a stationary hinge may forms at P_{I}, or a new traveling hinge H forms at P_{I} and moves in right or left directions, as shown in Fig. 3, until the hinge becomes inactive at P_{II}. In Phase III, $t \geqslant t_{\mathrm{II}}$, the beam moves as a rigid body, no plastic deformation occurs further.

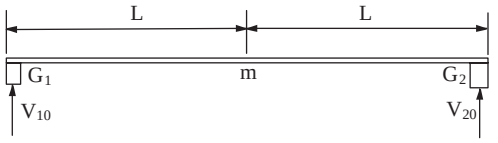

Fig. 1. A free–free beam subjected to impact at two free ends.

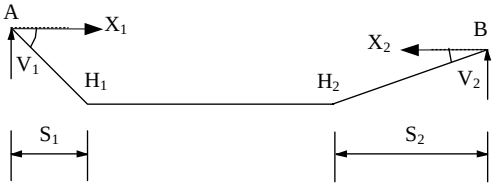

Fig. 2. Velocity diagram of the beam in Phase I.

2.1. Phase I: double traveling hinge phase ($0 \leqslant t \leqslant t_I$)

At the initial instant of impact two traveling hinges H_1 and H_2 form simultaneously at left and right ends of the beam respectively, and move toward each other. The velocity diagram of the beam is shown in Fig. 2, where V_1 and V_2 denote the velocities of the left free end A and right free end B, and $S_1 = AH_1$ and $S_2 = BH_2$ are the distances of the traveling hinges H_1 and H_2 to the impact points A and B, respectively.

Obviously segment H_1H_2 remains static in Phase I, and AH_1 may be regarded as a cantilever with free end A, and BH_2 as another cantilever with free end B. Both those cantilevers are struck at its free end by G_1 and G_2, respectively. It is well known that a r-p-p cantilever struck at its free end by a mass was first analyzed by Parkes (1955) and studied in more detail by the other researches (Johnson, 1972). With the help of Parkes' solution it is easy to obtain the analytical solutions in Phase I below.

For convenience, the following non-dimensional variables are introduced:

$$\begin{aligned}
&\xi = \frac{S_1}{L}, \quad \zeta = \frac{S_2}{L}, \quad \tau = t\sqrt{\frac{M_p}{mL^3}}, \quad e_{01} = \frac{G_1 V_{10}^2}{2M_p}, \quad e_{02} = \frac{G_2 V_{20}^2}{2M_p}, \quad (\dot{}) = \frac{d}{d\tau}(), \quad ()' = \frac{d}{dx}() \\
&v_1 = V_1\sqrt{mL/M_p}, \quad v_2 = V_2\sqrt{mL/M_p}, \quad v_{10} = V_{10}\sqrt{mL/M_p}, \quad v_{20} = V_{20}\sqrt{mL/M_p}, \quad g_1 = \frac{G_1}{mL} \\
&g_2 = \frac{G_2}{mL}, \quad \kappa_1 = k_1 L, \quad \kappa_2 = k_2 L, \quad x_1 = X_1/L, \quad x_2 = X_2/L, \quad w_1 = W_1/L, \quad w_2 = W_2/L
\end{aligned} \tag{1}$$

where M_p is the fully plastic bending moment of the beam, W_1 and W_2 are the transverse deflections of the beam, k_1 and k_2 are the curvatures in segment AH_1 and BH_2 respectively, and X_1 and X_2 are the coordinates along the beam with origins at A and B and positive directions indicated in Fig. 2, respectively.

The classical Parkes' solution gives that (Johnson, 1972)

$$v_1 = \frac{2g_1 v_{10}}{\xi + 2g_1} \tag{2}$$

$$\tau = \frac{g_1 v_{10}\xi^2}{3(\xi + 2g_1)} \tag{3}$$

$$v_2 = \frac{2g_2 v_{20}}{\zeta + 2g_2} \tag{4}$$

$$\tau = \frac{g_2 v_{20}\zeta^2}{3(\zeta + 2g_2)} \tag{5}$$

and the non-dimensional traveling speeds of hinge H_1 and H_2 are

$$\dot{\xi} = \frac{\mathrm{d}\xi}{\mathrm{d}\tau} = \frac{3(\xi + 2g_1)^2}{g_1 v_{10} \xi(\xi + 4g_1)} \tag{6}$$

and

$$\dot{\zeta} = \frac{\mathrm{d}\zeta}{\mathrm{d}\tau} = \frac{3(\zeta + 2g_2)^2}{g_2 v_{20} \zeta(\zeta + 4g_2)} \tag{7}$$

respectively. Eliminating τ between Eqs. (3) and (5) leads to

$$\left(\frac{\zeta}{\xi}\right)^2 \cdot \frac{\xi + 2g_1}{\zeta + 2g_2} = \frac{g_1 v_{10}}{g_2 v_{20}} \tag{8}$$

Eq. (8) provides a relationship between the positions of the two traveling hinges in the free–free beam. When $\xi + \zeta = 2$, the two traveling hinges H_1 and H_2 meet each other at point P_1 and Phase I ends. Subscript I pertains to the values at the end of Phase I below. Therefore, the non-dimensional coordinates ξ_I and ζ_I can be determined by solving following two equations

$$\left(\frac{\zeta_\mathrm{I}}{\xi_\mathrm{I}}\right)^2 \cdot \frac{\xi_\mathrm{I} + 2g_1}{\zeta_\mathrm{I} + 2g_2} = \frac{g_1 v_{10}}{g_2 v_{20}} \tag{9}$$

$$\xi_\mathrm{I} + \zeta_\mathrm{I} = 2 \tag{10}$$

For convenience of solving the above equations, the initial momentum ratio of the two strikers, c, is introduced,

$$c = \frac{g_1 v_{10}}{g_2 v_{20}} \tag{11}$$

A cubic algebraic equation is obtained from Eqs. (9) and (10),

$$(1 + c)\xi_\mathrm{I}^3 + 2[g_1 - 2 - c(1 + g_2)]\xi_\mathrm{I}^2 + 4(1 - 2g_1)\xi_\mathrm{I} + 8g_1 = 0 \tag{12}$$

The corresponding time τ_I as well as other quantities at the end of Phase I, such as the non-dimensional velocities $v_{1\mathrm{I}}$ and $v_{2\mathrm{I}}$ of the impact points A and B, can be obtained from Eqs. (2)–(4) as follows

$$\tau_\mathrm{I} = \frac{g_1 v_{10} \xi_\mathrm{I}^2}{3(\xi_\mathrm{I} + 2g_1)} \tag{13}$$

$$v_{1\mathrm{I}} = \frac{2g_1 v_{10}}{\xi_\mathrm{I} + 2g_1} \tag{14}$$

$$v_{2\mathrm{I}} = \frac{2g_2 v_{20}}{\zeta_\mathrm{I} + 2g_2} \tag{15}$$

The non-dimensional instantaneous curvature distributions along segments AH_1 and BH_2 at the end of Phase I are given by

$$\kappa_1(x) = w_1''(x) = \frac{2g_1^2 v_{10}^2 (x + 4g_1)}{3(x + 2g_1)^3} \quad 0 \leqslant x \leqslant \xi_\mathrm{I} \tag{16a}$$

$$\kappa_2(x) = w_2''(x) = \frac{2g_2^2 v_{20}^2 (x + 4g_2)}{3(x + 2g_2)^3} \quad 0 \leqslant x \leqslant \zeta_\mathrm{I} \tag{16b}$$

The rotation angles $\theta_1(x)$ and $\theta_2(x)$ of the cross-section along segments AH_1 and BH_2 respectively, can be obtained by integrating Eqs. (16) once with conditions of $\theta_1(\xi_I) = \theta_2(\zeta_I) = 0$. Thus,

$$\theta_1(x) = \frac{2g_1^2v_{10}^2(x+3g_1)}{3(x+2g_1)^2} - \frac{2g_1^2v_{10}^2(\xi_I+3g_1)}{3(\xi_I+2g_1)^2} \quad 0 \leqslant x \leqslant \xi_I \tag{17a}$$

$$\theta_2(x) = \frac{2g_2^2v_{20}^2(x+3g_2)}{3(x+2g_2)^2} - \frac{2g_2^2v_{20}^2(\zeta_I+3g_2)}{3(\zeta_I+2g_2)^2} \quad 0 \leqslant x \leqslant \zeta_I \tag{17b}$$

Integrating Eqs. (16) once more with conditions of $w_1(\xi_I) = w_2(\zeta_I) = 0$, the instantaneous deformed shape of the beam at the end of Phase I can be found to be

$$w_{1I}(x) = \frac{2}{3}g_1^2v_{10}^2\left[\ln\frac{x+2g_1}{\xi_I+2g_1} + \frac{(\xi_I+3g_1)(\xi_I-x)}{(\xi_I+2g_1)^2} - \frac{g_1(\xi_I-x)}{(\xi_I+2g_1)(x+2g_1)}\right] \quad 0 \leqslant x \leqslant \xi_I \tag{18a}$$

$$w_{2I}(x) = \frac{2}{3}g_2^2v_{20}^2\left[\ln\frac{x+2g_2}{\zeta_I+2g_2} + \frac{(\zeta_I+3g_2)(\zeta_I-x)}{(\zeta_I+2g_2)^2} - \frac{g_2(\zeta_I-x)}{(\zeta_I+2g_2)(x+2g_2)}\right] \quad 0 \leqslant x \leqslant \zeta_I \tag{18b}$$

The non-dimensional plastic work dissipated during Phase I is

$$e_{pI} = \frac{1}{2}g_1v_{10}^2 + \frac{1}{2}g_2v_{20}^2 - \frac{2g_1^2v_{10}^2(\xi_I+3g_1)}{3(\xi_I+2g_1)^2} - \frac{2g_2^2v_{20}^2(\zeta_I+3g_2)}{3(\zeta_I+2g_2)^2} \tag{19}$$

2.2. Phase II-1 general case: single traveling hinge mode ($t_I \leqslant t \leqslant t_{II}$)

After the two traveling hinges meet at point P_I in the beam, the subsequent response mode of the beam depends on both the concentrate masses and the initial speeds of the two strikers. Generally, a new single traveling plastic hinge H will form at point P_I and then move toward the striker that has smaller momentum at the end of Phase I. In the meantime, the beam remains in rigid body motion until the traveling hinge H becomes inactive. The velocity diagram is shown in Fig. 3, where $\dot{\varphi}_1$ and $\dot{\varphi}_2$ are the non-dimensional angular velocities of segments AH and BH, and the non-dimensional velocities at the impact points A and B are denoted by $\dot{u}_1$ and $\dot{u}_2$, respectively. The non-dimensional equations of motion are given by

$$\xi\left(\ddot{u}_1 - \frac{1}{2}\xi\ddot{\varphi}_1\right) = -g_1\ddot{u}_1 \tag{20a}$$

$$\xi^2\left(\frac{1}{2}\ddot{u}_1 - \frac{1}{3}\xi\ddot{\varphi}_1\right) = 1 \tag{20b}$$

for segment AH and

$$(2-\xi)\left[\ddot{u}_2 - \frac{1}{2}(2-\xi)\ddot{\varphi}_2\right] = -g_2\ddot{u}_2 \tag{21a}$$

$$(2-\xi)^2\left[\frac{1}{2}\ddot{u}_2 - \frac{1}{3}(2-\xi)\ddot{\varphi}_2\right] = 1 \tag{21b}$$

for segment HB, respectively. The continuity condition of transverse speed at hinge H requires that

$$\dot{u}_1 - \xi\dot{\varphi}_1 = \dot{u}_2 - (2-\xi)\dot{\varphi}_2 \tag{22}$$

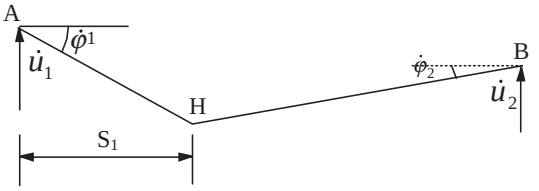

Fig. 3. Velocity diagram of the beam in Phase II.

Differentiating both sides of the above equation with respect to time, we have

$$\dot{\xi}(\dot{\varphi}_1+\dot{\varphi}_2)=\ddot{u}_1-\ddot{u}_2-\xi\ddot{\varphi}_1+(2-\xi)\ddot{\varphi}_2 \tag{23}$$

From Eqs. (20)–(23), $\ddot{u}_1$, $\ddot{u}_2$, $\ddot{\varphi}_1$, $\ddot{\varphi}_2$, $\dot{\varphi}_1$, $\dot{\varphi}_2$ and $\dot{\xi}$ can be expressed in terms of ξ as follows

$$\ddot{u}_1=-\frac{6}{\xi(\xi+4g_1)} \tag{24a}$$

$$\ddot{\varphi}_1=-\frac{9}{\xi^2(\xi+4g_1)}-\frac{3}{\xi^3} \tag{24b}$$

$$\ddot{u}_2=-\frac{6}{(2-\xi)(2-\xi+4g_2)} \tag{24c}$$

$$\ddot{\varphi}_2=-\frac{9}{(2-\xi)^2(2-\xi+4g_2)}-\frac{3}{(2-\xi)^3} \tag{24d}$$

$$\dot{\xi}(\dot{\varphi}_1+\dot{\varphi}_2)=\frac{3}{\xi(\xi+4g_1)}+\frac{3}{\xi^2}-\frac{3}{(2-\xi)(2-\xi+4g_2)}-\frac{3}{(2-\xi)^2} \tag{24e}$$

The initial conditions of Phase II can be obtained from the state of the end of Phase I as follows,

$$\begin{aligned}&\tau=\tau_{\mathrm{I}}: u_{1\mathrm{I}}=w_{1\mathrm{I}}(0),\ \ \dot{u}_{1\mathrm{I}}=v_{1\mathrm{I}},\ \ u_{2\mathrm{I}}=w_{2\mathrm{I}}(0),\ \ \dot{u}_{2\mathrm{I}}=v_{2\mathrm{I}}\\&\varphi_{1\mathrm{I}}=\theta_1(0),\ \ \dot{\varphi}_{1\mathrm{I}}=v_{1\mathrm{I}}/\xi_{\mathrm{I}},\ \ \varphi_{2\mathrm{I}}=\theta_2(0),\ \ \dot{\varphi}_{2\mathrm{I}}=v_{2\mathrm{I}}/\zeta_{\mathrm{I}}\end{aligned} \tag{25}$$

Combining Eqs. (24b) and (24d) and noting that $\frac{\mathrm{d}(\,)}{\mathrm{d}\tau}=\frac{\mathrm{d}(\,)}{\mathrm{d}\xi}\dot{\xi}$, it gives

$$\frac{\mathrm{d}(\dot{\varphi}_1+\dot{\varphi}_2)}{\mathrm{d}\xi}\cdot\dot{\xi}=-\frac{9}{\xi^2(\xi+4g_1)}-\frac{3}{\xi^3}-\frac{9}{(2-\xi)^2(2-\xi+4g_2)}-\frac{3}{(2-\xi)^3} \tag{26}$$

Substituting Eq. (24e) into the above equation, we have

$$\dot{\varphi}_1+\dot{\varphi}_2=\mathrm{e}^{\int F(\xi)\mathrm{d}\xi} \tag{27}$$

where

$$F(\xi)=\frac{2[(\xi+g_1)(2-\xi)^3(2-\xi+4g_2)+\xi^3(\xi+4g_1)(2-\xi+g_2)]}{(2-\xi)[\xi^3(\xi+4g_1)(2-\xi+2g_2)-\xi(2-\xi)^2(\xi+2g_1)(2-\xi+4g_2)]} \tag{28}$$

Therefore the speed of the traveling hinge H, $\dot{\xi}$, can be expressed in terms of variable ξ as follows

$$\dot{\xi}=\frac{f_1(\xi)}{\mathrm{e}^{\int F(\xi)\mathrm{d}\xi}} \tag{29}$$

where

$$f_1(\xi) = \frac{3}{\xi(\xi + 4g_1)} + \frac{3}{\xi^2} - \frac{3}{(2-\xi)(2-\xi+4g_2)} - \frac{3}{(2-\xi)^2} \tag{30}$$

Let $G(\xi) = \mathrm{e}^{\int F(\xi)\mathrm{d}\xi}/f_1(\xi)$, then Eqs. (24a)–(24d) can be solved by integration,

$$\dot{u}_1 = -\int \frac{6G(\xi)}{\xi(\xi+4g_1)}\,\mathrm{d}\xi \tag{31a}$$

$$u_1 = -\int \left[G(\xi)\int \frac{6G(\xi)}{\xi(\xi+4g_1)}\,\mathrm{d}\xi\right]\mathrm{d}\xi \tag{31b}$$

$$\dot{u}_2 = -\int \frac{6G(\xi)}{(2-\xi)(2-\xi+4g_2)}\,\mathrm{d}\xi \tag{31c}$$

$$u_2 = -\int \left[G(\xi)\int \frac{6G(\xi)}{(2-\xi)(2-\xi+4g_2)}\,\mathrm{d}\xi\right]\mathrm{d}\xi \tag{31d}$$

$$\dot{\varphi}_1 = -\int \frac{12(\xi+g_1)G(\xi)}{\xi^3(\xi+4g_1)}\,\mathrm{d}\xi \tag{31e}$$

$$\varphi_1 = -\int \left[G(\xi)\int \frac{12(\xi+g_1)G(\xi)}{\xi^3(\xi+4g_1)}\,\mathrm{d}\xi\right]\mathrm{d}\xi \tag{31f}$$

$$\dot{\varphi}_2 = -\int \frac{12(2-\xi+g_2)G(\xi)}{(2-\xi)^3(2-\xi+4g_2)}\,\mathrm{d}\xi \tag{31g}$$

$$\varphi_2 = -\int \left[G(\xi)\int \frac{12(2-\xi+g_2)G(\xi)}{(2-\xi)^3(2-\xi+4g_2)}\,\mathrm{d}\xi\right]\mathrm{d}\xi \tag{31h}$$

The integration constants in the integrating process can be determined by Eq. (25).

The deformation mechanism of single traveling hinge is valid until $\dot{\xi} = 0$, or $\dot{\varphi}_1 + \dot{\varphi}_2 = 0$, when the traveling hinge becomes inactive and then Phase II terminates. Let subscript II denote values at the end of Phase II below. Point P_{II} is the final position of the traveling hinge H and the non-dimensional coordinate of P_{II} is ξ_{II}. From Eq. (24e), ξ_{II} should satisfy a cubic algebraic equation as

$$(2+g_1+g_2)\xi_{\mathrm{II}}^3 - 2(3+4g_2-g_1)\xi_{\mathrm{II}}^2 + 4(1+2g_2-3g_1-4g_1g_2)\xi_{\mathrm{II}} + 8g_1(1+2g_2) = 0 \tag{32}$$

From Eq. (32) it is noted that the position of point P_{II} is only dependent on g_1 and g_2, and independent on the impact speeds of both strikers.

During the response process in Phase II, the curvature of those regions, where the traveling hinge H has passed through, will be increased while the curvature of the other regions remains unchanged. The magnitude of the curvature produced in Phase II is obtained as follows

$$\kappa = (\dot{\varphi}_1 + \dot{\varphi}_2)/\dot{\xi} = \mathrm{e}^{2\int F(\xi)\mathrm{d}\xi}/f_1(\xi) \tag{33}$$

Therefore the total permanent curvature of the beam should be the sum of those produced in Phase I and Phase II respectively.

Finally the energy dissipation during Phase II can be obtained as follows

$$e_{\mathrm{pII}} = (\varphi_{1\mathrm{II}} + \varphi_{2\mathrm{II}}) - e_{\mathrm{pI}} \tag{34}$$

2.3. Phase II-2 a particular case: single stationary hinge mode ($t_I \leqslant t \leqslant t_{II}$)

Except the general case described above, however, there is a particular case. In this case, instead of a traveling hinge deformation mechanism, a single stationary hinge mode is valid in Phase II, when the mass g_1, g_2 and the ratio of initial momentum of the two strikers, c, satisfy a condition (see Eq. (37) below). For example if $g_1 = g_2$ and $c = 1$, then intuitively a stationary plastic hinge will form at mid-span cross-section in Phase II and the subsequent response is that each half of the beam rotates about the stationary hinge as a rigid-body until the angular speeds of them decrease to zero. Actually, if the root of Eq. (12), which determines the meeting position of the two traveling hinges at the end of Phase I, equals to the root of Eq. (32), which determines the final position of the traveling hinge at the end of Phase II, it indicates that both P_{I} and P_{II} are at the same position. This is the particular case for which only a stationary

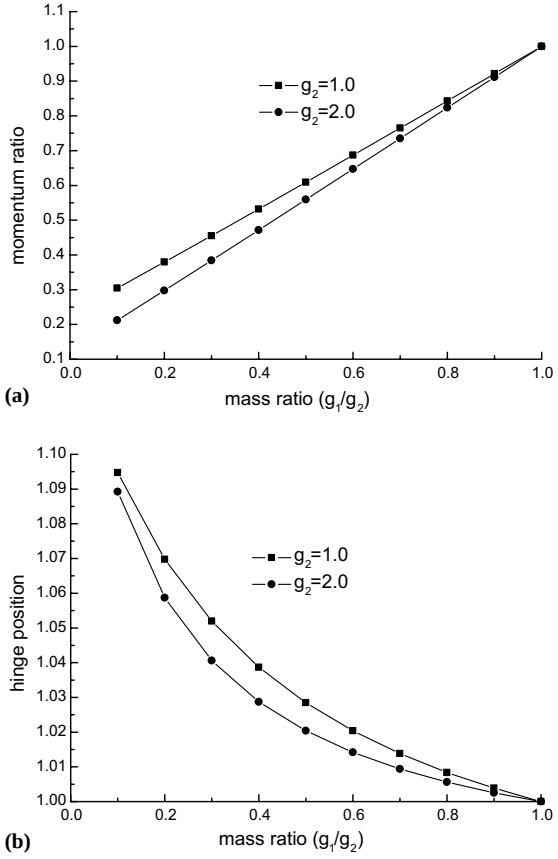

Fig. 4. The condition of forming a single stationary hinge in Phase II: (a) mass ratio versus initial momentum ratio; (b) hinge position versus mass ratio.

hinge deformation mechanism is valid in Phase II. Thus from Eqs. (9), (10) and (24e), the condition can be found as

$$\left(\frac{2-\xi_{\mathrm{I}}}{\xi_{\mathrm{I}}}\right)^2 \cdot \frac{\xi_{\mathrm{I}}+2g_1}{2-\xi_{\mathrm{I}}+2g_2} = c \tag{35}$$

$$\frac{\xi_{\mathrm{I}}+2g_1}{\xi_{\mathrm{I}}^2(\xi_{\mathrm{I}}+4g_1)} = \frac{2-\xi_{\mathrm{I}}+2g_2}{(2-\xi_{\mathrm{I}})^2(2-\xi_{\mathrm{I}}+4g_2)} \tag{36}$$

Eliminating ξ_{I} from Eqs. (35) and (36) gives

$$\frac{c-g_1+cg_1+2cg_2}{1-cg_2+g_2+2g_1} \cdot \left(\frac{1-2cg_2+2g_1}{c+2cg_2-2g_1}\right)^2 - c = 0 \tag{37}$$

The above equation is the condition for the beam to have a single stationary hinge mode in Phase II. When $g_2 = 1.0$ and 2.0, the relationships between the striker masses g_1, g_2 and the initial momentum ratio c are shown in Fig. 4(a), and the positions of the stationary hinge are shown in Fig. 4(b).

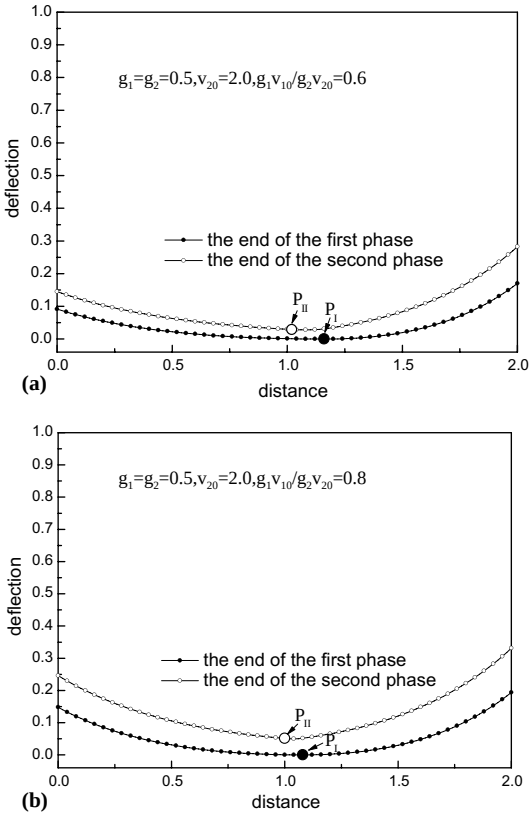

Fig. 5. The deformed shapes of the beam at the ends of Phase I and II, for $g_1 = g_2$: (a) $g_1 = g_2 = 0.5$, $v_{20} = 2.0$, $c = 0.6$; (b) $g_1 = g_2 = 0.5$, $v_{20} = 2.0$, $c = 0.8$.

For this case, Fig. 3 can also be adopted to show the velocity diagram in Phase II, provided H indicates the stationary hinge. Similar to the analysis in previous section, and noting that $\dot{\xi} \equiv 0$ and ξ is a constant, $\xi = \xi_{\mathrm{I}}$, the following important results can be obtained.

(1) At the end of Phase II the total rotation at the stationary hinge H is given by

$$\theta_{\mathrm{hII}} = \theta_{\mathrm{h1II}} + \theta_{\mathrm{h2II}} = \left[\frac{g_1 v_{10}}{\xi_{\mathrm{I}}(\xi_{\mathrm{I}} + 2g_1)} + \frac{g_2 v_{20}}{\zeta_{\mathrm{I}}(\zeta_{\mathrm{I}} + 2g_2)}\right]^2 \Bigg/ 6\left[\frac{\xi_{\mathrm{I}} + g_1}{\xi_{\mathrm{I}}^3(\xi_{\mathrm{I}} + 4g_1)} + \frac{\zeta_{\mathrm{I}} + g_2}{\zeta_{\mathrm{I}}^3(\zeta_{\mathrm{I}} + 4g_2)}\right] \tag{38}$$

where θ_{h1II} and θ_{h2II} are the rotations of segment AH and BH about the stationary hinge, H, respectively, and are given by

$$\theta_{\mathrm{h1II}} = \frac{g_1 v_{10}}{\xi_{\mathrm{I}}(\xi_{\mathrm{I}} + 2g_1)}\left[\frac{g_1 v_{10}}{\xi_{\mathrm{I}}(\xi_{\mathrm{I}} + 2g_1)} + \frac{g_2 v_{20}}{\zeta_{\mathrm{I}}(\zeta_{\mathrm{I}} + 2g_2)}\right] \Bigg/ 6\left[\frac{\xi_{\mathrm{I}} + g_1}{\xi_{\mathrm{I}}^3(\xi_{\mathrm{I}} + 4g_1)} + \frac{\zeta_{\mathrm{I}} + g_2}{\zeta_{\mathrm{I}}^3(\zeta_{\mathrm{I}} + 4g_2)}\right]$$

$$\theta_{\mathrm{h2II}} = \frac{g_2 v_{20}}{\zeta_{\mathrm{I}}(\zeta_{\mathrm{I}} + 2g_2)}\left[\frac{g_1 v_{10}}{\xi_{\mathrm{I}}(\xi_{\mathrm{I}} + 2g_1)} + \frac{g_2 v_{20}}{\zeta_{\mathrm{I}}(\zeta_{\mathrm{I}} + 2g_2)}\right] \Bigg/ 6\left[\frac{\xi_{\mathrm{I}} + g_1}{\xi_{\mathrm{I}}^3(\xi_{\mathrm{I}} + 4g_1)} + \frac{\zeta_{\mathrm{I}} + g_2}{\zeta_{\mathrm{I}}^3(\zeta_{\mathrm{I}} + 4g_2)}\right]$$

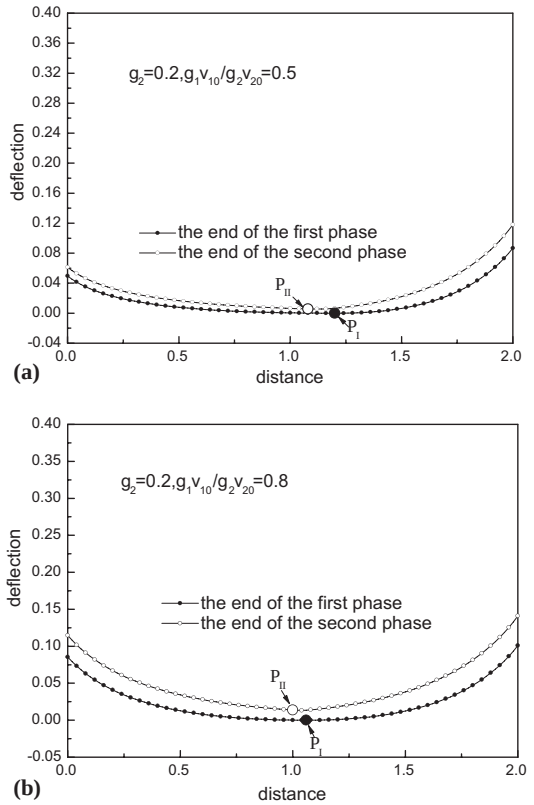

Fig. 6. The deformed shapes of the beam at the ends of Phase I and II, for $g_1 \neq g_2$: (a) $g_2 = 0.2$, $c = 0.5$; (b) $g_2 = 0.2$, $c = 0.8$.

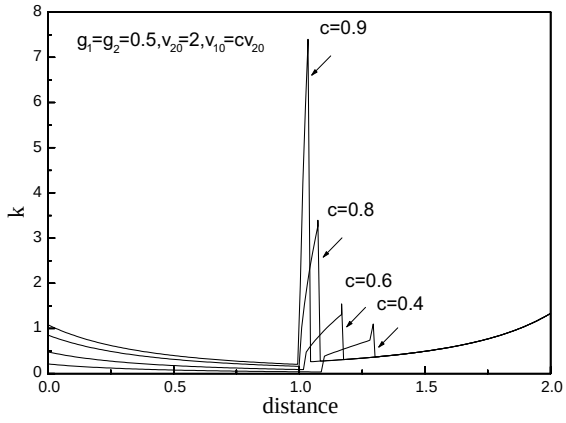

Fig. 7. Curvature distributions of the deformed beam for various c with $g_1 = g_2$.

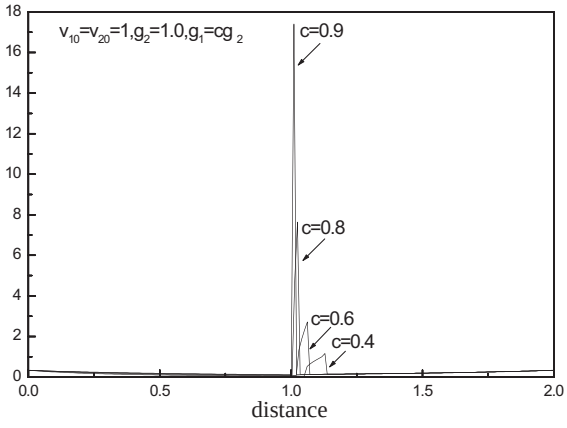

Fig. 8. Curvature distributions of the deformed beam for various c with $v_{10} = v_{20}$.

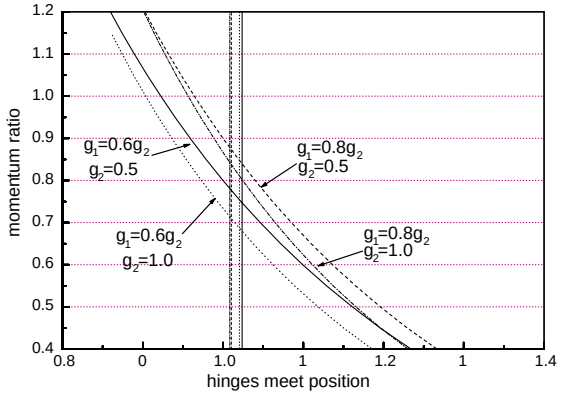

Fig. 9. Relationship between failure position and initial momentum ratio.

Table 1
Comparison for the failure predictions between present model and FEM analysis

Case		Symmetric impact	Unsymmetric impact (traveling hinge in Phase II)	Unsymmetric impact (stationary hinge in Phase II)
g_1		1.0	1.0	0.2
g_2		1.0	1.0	1.0
v_1 (m/s)		30	24	75.85
v_2 (m/s)		30	40	40
c		1.0	0.6	0.38
ξ_{I}	e-p-p	1.0	1.1	1.04
	r-p-p	1.0	1.15	1.07
ξ_{II}	e-p-p	1.0	–	1.04
	r-p-p	1.0	1.0	1.07
θ	e-p-p	0.29	0.21	0.31
	r-p-p	0.30	0.22	0.34
t_{I} (ms)	e-p-p	4.5	4.0	6.0
	r-p-p	6.0	6.0	7.0
t_{II} (ms)	e-p-p	14.0	14.5	14.0
	r-p-p	13.5	14.3	14.0

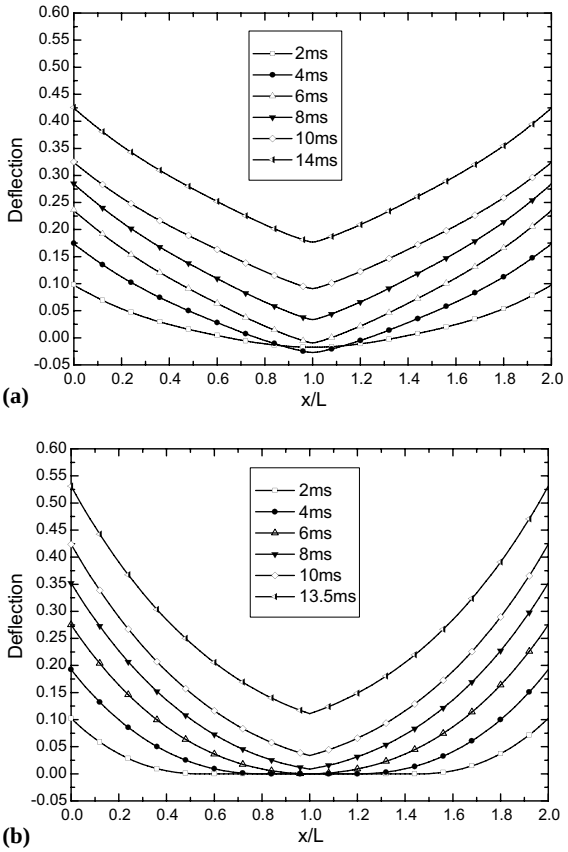

Fig. 10. Instant deformation profiles of symmetric impact for $c = 1$ and $g_1 = g_2$: (a) e-p-p model by FEM; (b) r-p-p model.

(2) At the end of Phase II the transverse displacement of section H is given by

$$w_{\mathrm{hII}} = \frac{\xi_{\mathrm{I}} + 2g_1}{12\xi_{\mathrm{I}}^2(\xi_{\mathrm{I}} + 4g_1)} \left[\frac{\dfrac{g_1 v_{10}}{\xi_{\mathrm{I}}(\xi_{\mathrm{I}} + 2g_1)} + \dfrac{g_2 v_{20}}{\zeta_{\mathrm{I}}(\zeta_{\mathrm{I}} + 2g_2)}}{\dfrac{\xi_{\mathrm{I}} + g_1}{\xi_{\mathrm{I}}^3(\xi_{\mathrm{I}} + 4g_1)} + \dfrac{\zeta_{\mathrm{I}} + g_2}{\zeta_{\mathrm{I}}^3(\zeta_{\mathrm{I}} + 4g_2)}} \right]^2 \tag{39}$$

(3) The deflections of AH and BH at the end of Phase II are

$$w_{1\mathrm{II}}(x) = w_{1\mathrm{I}}(x) + w_{\mathrm{hII}} + (1 - x)\theta_{\mathrm{h1II}} \quad 0 \leqslant x \leqslant \xi_{\mathrm{I}} \tag{40}$$

$$w_{2\mathrm{II}}(x) = w_{2\mathrm{I}}(x) + w_{\mathrm{hII}} + (1 - x)\theta_{\mathrm{h2II}} \quad 0 \leqslant x \leqslant \zeta_{\mathrm{I}} \tag{41}$$

2.4. Phase III: rigid body motion ($t > t_{II}$)

When $t > t_{\mathrm{II}}$, the beam continues moving as a rigid body, and neither plastic dissipation nor deformation takes place further.

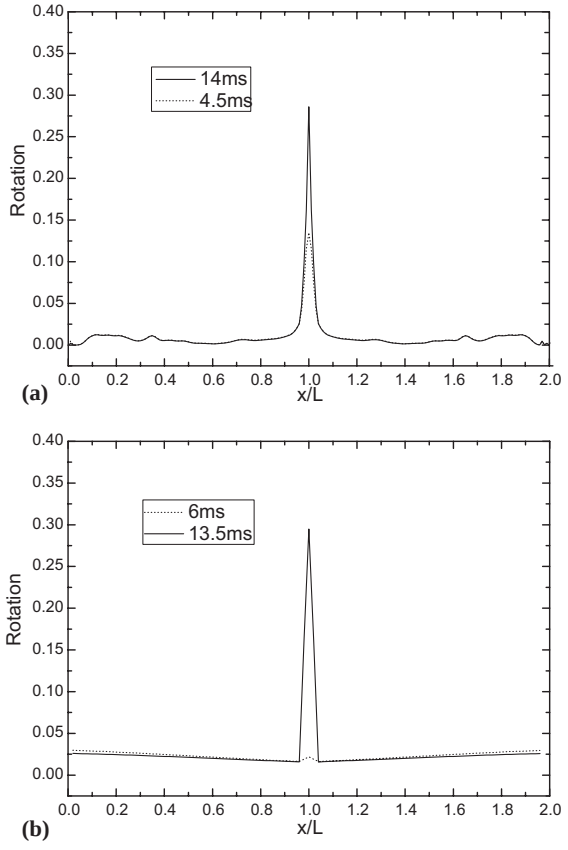

Fig. 11. Instant cross-section rotation distributions of symmetric impact for $c = 1$ and $g_1 = g_2$: (a) e-p-p model by FEM; (b) r-p-p model.

3. Simplified plastic failure analysis for the free–free beam

3.1. Plastic deformation of the beam

It is seen from Eq. (12) that the position of point P_I depends on the masses g_1, g_2 and initial momentum ratio c, which are adopted as non-dimensional parameters in the calculation. The deformed profiles of the beam at the end of Phase I and II are shown in Figs. 5 and 6, in which the big black and white circles are used to denote the positions of P_I and P_{II} respectively. Besides, it may be observed in Figs. 5 and 6 that when $c < 1.0$, P_I is located on the right side of mid-span of the beam, and single traveling hinge H moves back to the left side of P_I in Phase II and finally vanishes at P_{II} for both cases of $g_1 = g_2$ and $g_1 \neq g_2$.

3.2. Approximate estimation of breakup section of the free–free beam

Present r-p-p model can be adopted to predict the possibility of the bending failure of a free–free beam subjected to impact at its two free ends by concentrated moving masses. This is because the bending failure would be understood as a concentrated high curvature region caused by plastic hinge formation.

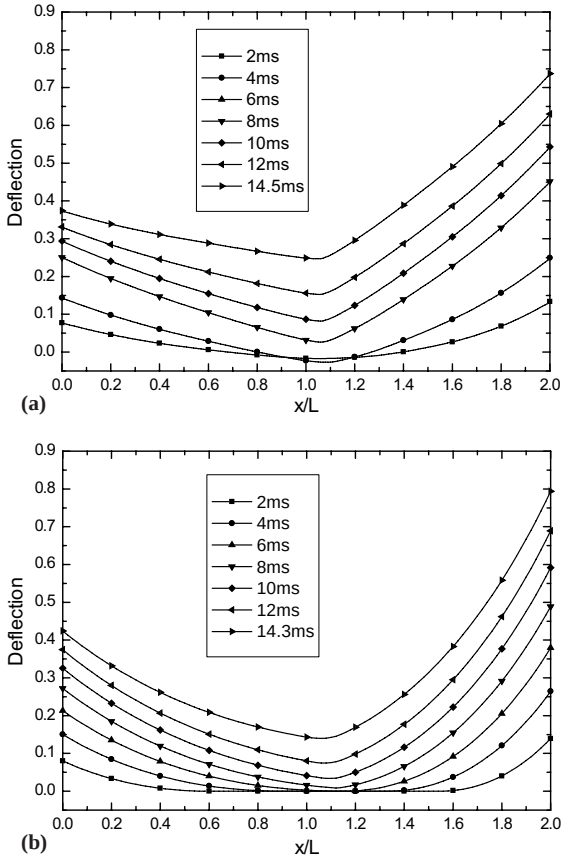

Fig. 12. Instant deformation profiles of unsymmetrical impact, a general case with $c = 0.6$: (a) e-p-p model by FEM; (b) r-p-p model.

In the previous sections, it is shown that there are two possible deformation mechanisms in Phase II, i.e. a single traveling hinge or a single stationary hinge. Which mechanism governs the dynamic response of the beam depends on the mass g_1 and g_2 as well as the initial momentum ratio c. The condition of Eq. (37) has been established to examine the deformation mode which governs in Phase II actually. In most cases, g_1, g_2 and c do not happen to satisfy Eq. (37), therefore single traveling hinge mechanism governs most frequently in Phase II for the impinged free–free beam.

When $g_1 = g_2 = 0.5$, $v_{20} = 2$ and c taken from 0.4 to 0.9, Fig. 7 shows the permanent curvature distributions along the beam. It is observed in Fig. 7 that there are significant high curvature regions which are located between P_{I} and P_{II}. The maximum value of the curvature which is observed at point P_{I} reaches $\kappa \approx 7.4$, 3.5, 1.5 and 1.2 for the parameter c taken to be 0.9, 0.8, 0.6 and 0.4, respectively. This indicates that the high curvature region is in segment $P_{\mathrm{I}}P_{\mathrm{II}}$, where is the most liable breakup region.

When $v_{10} = v_{20} = 1.0$, $g_2 = 1.0$ and c taken from 0.4 to 0.9, Fig. 8 shows the permanent curvature distributions along the beam. In comparison with Fig. 7, it is observed that for the same initial momentum ratio c, the high curvature regions in Fig. 8 are smaller than that in Fig. 7 and concentrate on the neighborhood of point P_{I}. Furthermore the absolute maximum values of the non-dimensional curvature in Fig. 8 are about two times of those in Fig. 7. This indicates that for the same initial momentum the heavier striker is liable to result in breakup of the beam.

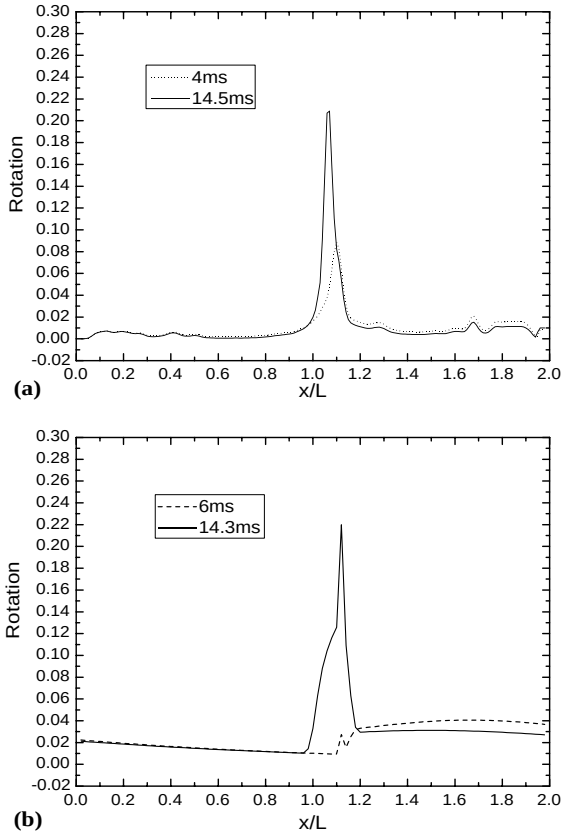

Fig. 13. Instant cross-section rotation distributions of unsymmetrical impact, a general case with $c = 0.6$: (a) e-p-p model by FEM; (b) r-p-p model.

It is dangerous case leading to breakup of the beam when a given set of parameters g_1, g_2 and c satisfies Eq. (37) and the single stationary hinge mechanism governs in Phase II. For this case the bending failure of the free–free beam is caused by an excessive rotation at stationary hinge cross-section where the curvature tends to be infinite large based on r-p-p mode and it is inappropriate to adopt the curvature as the critical rupture parameter of the beam.

The curves of the non-dimensional coordinate of point P_{I} which depend on g_1, g_2 and c, are determined by Eq. (12), shown in Fig. 9. In order to show more clearly the relationship between the two deformation mechanisms, the curves given by Eq. (32) for the position of point P_{II} which depend only on g_1 and g_2 are also shown in Fig. 9 as straight vertical lines. The intersect points of the two sets of curves represent the particular case, for which g_1, g_2 and c satisfy Eq. (37) and the single stationary hinge mode governs in Phase II.

3.3. Typical examples and comparison with FEM based on elastic–plastic material model

One of the important issues which should be addressed is how large the difference will be for the predictions of breakup cross-section positions of the beam between present simplifying approach based on the r-p-p model and the FEM dynamic analysis based on elastic perfectly plastic (e-p-p) material model. For

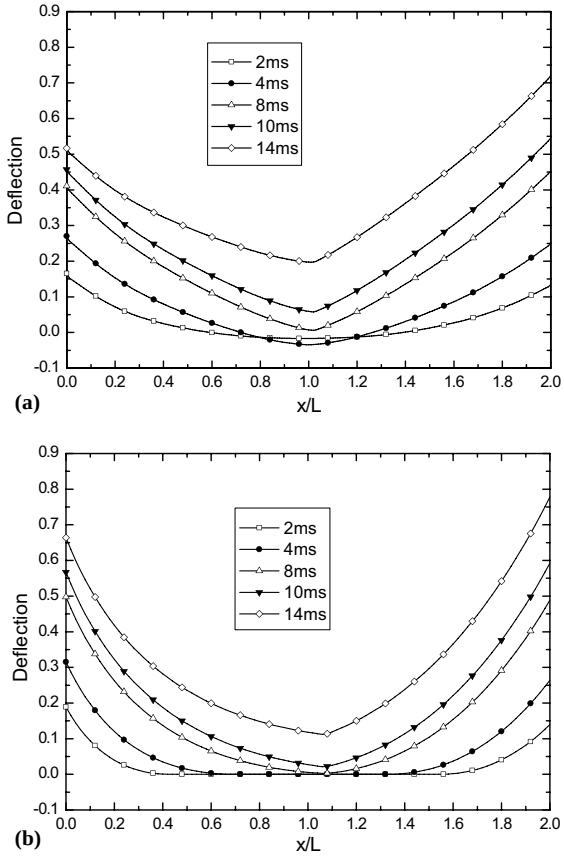

Fig. 14. Instant deformation profiles for the case of stationary hinge formed in Phase II: (a) e-p-p model by FEM; (b) r-p-p model.

the purpose of addressing the problem, as an example a mild steel free–free beam subjected to impact at both left and right free ends has been analyzed based on the r-p-p model by the theoretical approach suggested in present paper and the e-p-p model by FEM code from MSC/Dytran (The MacNeal-Schwendler Corporation, 1996). The beam is 1000 mm in length, and rectangular cross-section with 20 mm in thickness and 40 mm in width, and the yield stress and Young's modulus for the mild steel material are 220 MPa and 210 GPa, respectively.

Three different impact cases are considered below, i.e. one symmetric impact and two unsymmetrical impacts, see Table 1 for the impact parameters. For the unsymmetrical impacts, one is the case with single traveling hinge in Phase II and the other is with single stationary hinge in Phase II, which has been analyzed in previous sections. The results, such as instantaneous profiles and rotation distributions of the deformed beam predicted by present simplified theoretical approach based on r-p-p model and by FEM simulation based on e-p-p model, are all shown in Figs. 10–15. Some important results of the comparison between the predictions of the two models are shown in Table 1. The following characteristics can be observed.

(i) For the case of symmetric impact it implies that both left and right free ends of the beam are subjected to identical initial momentum ($c = g_1 v_{10}/g_2 v_{20} = 1$) with $g_1 = g_2$. Both the e-p-p and the r-p-p model predict there is a sharp peak in rotation distribution at the middle-span of the beam, see Fig. 11. The

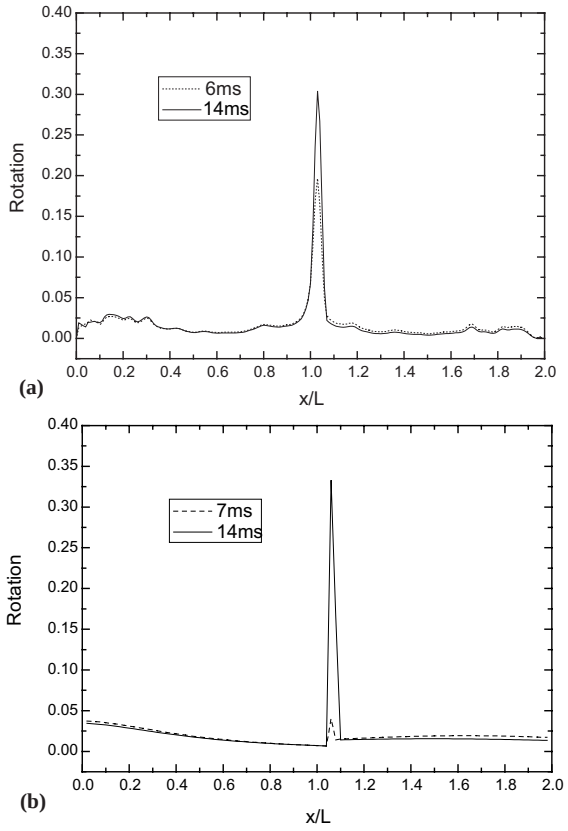

Fig. 15. Instant cross-section rotation distribution for the case of stationary hinge formed in Phase II: (a) e-p-p model by FEM; (b) r-p-p model.

possible breakup position and the maximum value of the permanent rotation predicted by present approach based on the r-p-p and by FEM based the e-p-p model are in good agreement, as shown in Figs. 10 and 11.

(ii) For the case of unsymmetrical impact with single traveling hinge in Phase II, it implies that it is a general impact condition with $c = g_1 v_{10}/g_2 v_{20} \neq 1$. Both the e-p-p and the r-p-p model predict there is a large rotation region between $x/L = 1.0$ and 1.2 on the right side of the mid-span of the beam. The maximum value of the permanent rotation in the region predicted by present approach based on the r-p-p model is good in agreement with that predicted by FEM based on the e-p-p model, as shown in Figs. 12 and 13.

(iii) For the case of unsymmetrical impact with single stationary hinge in Phase II, it implies that the relation between initial momentum ratio, c, mass g_1 and g_2 satisfy Eq. (37). Both the e-p-p and the r-p-p models predict there is a sharp peak in rotation distribution at the stationary hinge position, which is about $x/L = 1.04$ on the right side of the mid-span of the beam. The possible breakup position and the maximum value of the permanent rotation predicted by present approach based on the r-p-p model is good in agreement with those predicted by FEM based on the e-p-p model as shown in Figs. 14 and 15.

4. Conclusion

The main interest of the present study is to predict the dynamic plastic failure behavior of a free–free beam subjected to impact at both left and right free ends. In order to search a simple model to estimate approximately the most liable breakup cross-section of the beam, a rigid, perfectly plastic material idealization was adopted. This leads to the present formulations with closed form solutions, which in some particular situations can be expressed in an extremely simple equation to determine the possible breakup cross-section in the beam. The following conclusions are supported:

(1) The dynamic plastic response of the free–free beam consists two phases, i.e. the double traveling hinge phase and single traveling (or stationary) hinge phase. For both phases, the complete solutions, which satisfy the equations of motion, the boundary conditions and the initial conditions for the problem, are obtained. Therefore, the permanent deformation, rotation and curvature of the beam can be predicted by use of present r-p-p model.

(2) Two important parameters are obtained. They are the coordinates of point P_{I} where the two traveling hinges meet at the end of Phase I, and point P_{II} where the single traveling hinge becomes inactive at the end of Phase II. The former ξ_{I}, which depends on masses g_1, g_2 and ratio of initial momentum, c, can be determined by a cubic algebraic Eq. (12) and it is found that the maximum curvature appears at this position. Therefore the most liable breakup cross-section of the beam will be at this position. The latter ξ_{II}, which only depends on mass g_1 and g_2, can be determined by Eq. (32). It is found that a significant high curvature region, which is quite narrow, will appear between P_{I} and P_{II} Therefore this narrow region in the beam, as it undergoes a serious local deformation caused by high curvature, will be liable to be broken up mostly as well.

(3) Employing MSC-Dytran, a commercial FEM code, and elastic–plastic material assumption, it is verified that there is a large rotation region during the dynamic response in the beam and the location of the region is agree well with that predicted by analytical solutions based on present r-p-p model. Therefore the possible breakup cross-section predicted by present paper can be adopted approximately as design parameter for evaluation of the dynamic strength of a free–free beam subjected to impact by moving concentrated mass at two free ends.

Acknowledgements

The work described in this article was supported by the National Natural Science Foundation of China (grant number 10272011). The authors gratefully acknowledge the support.

References

Ahmed, T.U., Ramachandra, L.S., Bhattacharyya, S.K., 2001. Elasto-plastic response of free–free beams subjected to impact loads. Int. J. Impact Eng. 25, 661–681.

Johnson, W., 1972. Impact strength of materials. Edward Arnold Ltd.

Jones, N., Wierzbicki, T., 1987. Dynamic plastic failure of a free–free beam. Int. J. Impact Eng. 6, 240–255.

Lee, E.H., Symonds, P.S., 1952. Large plastic deformations of beam under transverse impact. J. Appl. Mech. 19, 308–314.

Parkes, E.W., 1955. The permanent deformation of a cantilever struck transversely at its tip. Proc. R. Soc. London, Ser. A 228, 462–476.

Symonds, P.S., 1953. Dynamic load characteristics in plastic bending of beams. J. Appl. Mech. 20, 475–481.

Symonds, P.S., 1967. Survey of methods of analysis for plastic deformation of structure under dynamic loading. Brown University, Division of Engineering Report BU/NSRDC/, pp. 1–67.

Symonds, P.S., 1985. A review of elementary approximation techniques for plastic deformation of pulse-loaded structures. In: Reid, S.R. (Ed.), Metal forming and impact mechanics. Oxford, Pergamon Press, pp. 175–194.

Symonds, P.S., Frye, C.W.G., 1988. On the relation between rigid-plastic and elastic–plastic predictions of response to pulse loading. Int. J. Impact Eng. 7, 139–149.

Symonds, P.S., Leth, C.F.A., 1954. Impact of finite beam of ductile metal. J. Appl. Mech. 2, 92–102.

The MacNeal-Schwendler Corporation, 1996. MSC/DYTRAN User's Manual.

Woodward, R.L., Baxtex, B.J., 1986. Experiments on the impact bending of continuous and notched steel beams. Int. J. Impact Eng. 4, 57–68.

Yang, J.L., Yu, T.X., Reid, S.R., 1998. Dynamic behavior of a rigid perfectly plastic free–free beam subjected to step-loading at any cross-section along its span. Int. J. Impact Eng. 21 (3), 165–175.

Yang, J.L., Xi, F., 2000. Dynamic response of an elastic–plastic free–free beam subjected to impact at any cross-section along its span. Key Eng. Mater. 177 (1), 273–278.

Yu, T.X., Yang, J.L., Reid, S.R., Austin, C.D., 1996. Dynamic behavior of elastic–plastic free–free beams subjected to impulsive loading. Int. J. Solids Struct. 33, 2659–2680.

Yu, T.X., Yang, J.L., Reid, S.R., 2000. Deformable body impact: dynamic plastic behaviour of moving free–free beams striking the tip of a cantilever beam. Int. J. Solids Struct. 38, 261–287.